

Effect of particle size on the photocatalytic activity of BiNbO₄ under visible light irradiation

S P Adhikari^{1,2} and A Lachgar^{1,2}

¹Department of Chemistry, Wake Forest University, Winston Salem, NC 27109, USA

²Center for Energy, Environment and Sustainability, Wake Forest University, Winston Salem, NC 27109, USA

Email: lachgar@wfu.edu

Abstract

Numerous attempts have focused on developing more efficient visible-light active photocatalysts. Bismuth niobate (BiNbO₄) was reported as a potential candidate for photocatalytic water splitting and for the degradation of organic molecule under visible-light irradiation because of its small band gap and appropriate band positions. Here, three BiNbO₄ samples with different, uniform particle sizes were synthesized. The effect of BiNbO₄ particle size on its photocatalytic activity was studied by using the reduction of 4-nitroaniline as model reaction. Results show that the photocatalytic degradation of 4-nitroaniline varies systematically with the change in particle size and surface areas. To better understand the correlation between structure, composition, morphology, and optical properties, the catalysts were characterized by transmission electron microscopy (TEM), scanning electron microscope (SEM), Powder X-ray diffraction (PXRD), Brunauer-Emmett-Teller (BET) surface area, UV-vis diffuse reflectance spectroscopy (DRS), and photoluminescence spectroscopy (PL).

Key Words: Photocatalysis, Particle size, Surface area, Bismuth niobate

1. Introduction

Semiconductor based photocatalytic processes are widely recognized as viable solutions to current environmental problems and clean energy generation [1]. After the discovery of titanium dioxide (TiO₂) as an ultraviolet light active photocatalyst for water splitting and degradation of organic compounds in the early 1970's, a large number of semiconductors have been reported to be active for energy generation and environmental applications [2,3]. Most semiconductors explored to date have large band gaps, thus require UV light irradiation to induce catalytic activity. However, solar energy consists mainly of visible (~45 %) and infrared light (~50 %) with a small contribution of UV light (~5 %). To more efficiently utilize solar energy irradiation, photocatalysts must show good activity under visible light irradiation (400 nm < λ < 800 nm) with a band gap less than 3 eV [4–7]. In addition, the quantum efficiency is negatively affected by thermodynamically favored recombination of photogenerated electron-hole pairs. Also, many semiconductor photocatalysts, chalcogenides in particular, undergo degradation under solar energy due to the photo-corrosion [8]. Therefore, there is a significant need to develop visible-light active photocatalysts with high activity and good chemical and physical stability.

To overcome the limitation that a majority of oxide-based photocatalysts are only UV responsive, many methods have been developed to extend their light absorption range into the visible region, such as doping with metal or non-metal ions or forming semiconductors heterojunctions by combining two or three semiconductors [9–17]. Other methods for enhancing the activity of given catalyst by allowing better separation of the photogenerated carriers have been explored. Some of these approaches include the addition of sacrificial reagents, cocatalyst loading, and preparing materials with higher active sites densities [1,4,18–20]. Another interesting approach is the reduction of grain size to decrease the time necessary for the charge carriers to migrate to the surface of the particle and be involved in



electrochemical reactions. It is well known that for randomly generated charge carriers, the average diffusion time from bulk to the surface is given by $\tau = r^2/\pi^2 D$, where r is the grain radius and D is the diffusion coefficient of the carrier [21]. Therefore, when the grain radius decreases, the diffusion time is reduced and the migration of the charge carriers to the surface of the particles is facilitated. The preparation of particles with small and uniform size is one of the key issues to address the photocatalytic activity of different materials [4,18,22–24]. Conventional high temperature solid-state synthetic methodologies generally lead to rather large particle size due to sintering, and small surface area. Synthesis methods using mild temperatures and solvents, on the other hand, has significant advantages in terms of homogeneity, low temperature and control over particle size, leading to higher surface area that can enhance the overall photocatalytic activity [4,18,25,26].

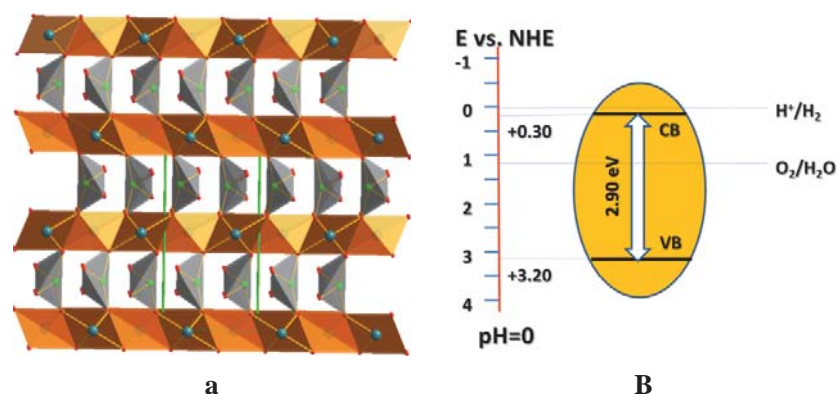


Figure 1: (a) Crystal structure representation of BiNbO₄. (b) Band gap and calculated band positions of BiNbO₄. The conduction band (CB) bottom (E_{CB}) was calculated empirically according to the formula, $E_{CB} = X - 0.5E_g + E_0$, where E_g is the band gap energy, E_0 is a scale factor relating the reference electrode's redox level to the absolute vacuum scale ($E_0 = 4.5$ eV for normal hydrogen electrode), and X is the electronegativity of the semiconductor, which can be expressed as the geometric mean of the absolute electronegativity of the constituent atoms. The value of X for BiNbO₄ was taken as 6.26 eV for the calculation)

Bismuth niobate (BiNbO₄) was reported to be photocatalytically active for water splitting and organic molecule degradations using sunlight [27–29]. Figure 1 show the crystal structure of orthorhombic phase of BiNbO₄, where both the Bi and Nb are coordinately bonded to the six neighboring oxygen atoms. Several band-gap engineering approaches such as anion and cation doping and dye sensitization were investigated to make BiNbO₄ photocatalytically active in the visible light region [29–33]. Zou et al. reported a novel series of Solid Photocatalysts, BiTa_{1-x}Nb_xO₄ ($0 \leq x \leq 1$) for water splitting [34]. The same group demonstrated the potential of Bi₂MNbO₇ (M= Al, Ga, In) as catalyst to split water into hydrogen and oxygen under both ultraviolet and visible light [28]. Most photocatalysts based on these studies are synthesized by the solid-state synthetic methodology at high temperature, leading to large particle size and small surface areas. Still, some recent papers have reported a wet chemical route to synthesize bismuth and niobium metals based oxides [35–39]. Here, we report the preparation of BiNbO₄ with different particle sizes and surface areas using different wet chemistry methods, and the study of their photocatalytic activity towards the reduction of 4-nitroaniline using visible light irradiation ($\lambda \geq 400$ nm). The results are compared with that of the compound synthesized by solid-state reaction method to correlate the activities with particle sizes and surface areas.

2. Experimental Section

2.1 Synthesis

All solvents and chemicals used were reagent-grade quality and were used without further purification. Bismuth Oxide (99.8%) and Niobium Chloride (99.9%) were purchased from Alfa Aesar (USA). Niobium Oxide (99.9%) and Triblock Copolymer Surfactant Pluronic P123 ($\text{HO}(\text{CH}_2\text{CH}_2\text{O})_{20}(\text{CH}_2\text{CH}(\text{CH}_3)\text{O})_{70}(\text{CH}_2\text{CH}_2\text{O})_{20}\text{H}$) were obtained from Sigma Aldrich (USA). Three different preparation methods were performed including high temperature solid state reaction method. In a typical solid-state reaction method (**S1**), 2.5 mmol Bismuth oxide (Bi_2O_3) and 2.5 mmol Niobium oxide (Nb_2O_5) were mixed and ground manually in an agate mortar to obtain fine powder[40]. The mixture was heated to 900 °C at a rate of 5 °C/min and the temperature was held at 900 °C for 24 hours then cooled to room temperature at the rate of 10 °C/min to produce light yellow microcrystalline powder of pure BiNbO_4 as determined by powder X-ray diffraction (PXRD). BiNbO_4 was also synthesized by solution method using P123 as surfactant (**S2**)[41]. In a typical synthesis, 2.5 mmol Bismuth nitrate pentahydrate and 2.5 mmol Niobium chloride were separately dissolved in 10 ml of ethanol and stirred for 0.5 hr. A solution of 1.0 gm of P123 dissolved in 10 ml of ethanol was also prepared. The three solutions were mixed and stirred to obtain a colorless translucent solution, which was aged for 48 hours at room temperature then dried at 80 °C to remove excess ethanol. The dry mass was calcined at 750 °C at the rate of 5 °C/min and held at this temperature for 12 hours. The temperature of calcination was determined from thermogravimetric analysis (TGA).

BiNbO_4 was also synthesized by two-step hydrothermal process (**S3**). The first step was carried out to prepare niobic acid ($\text{Nb}_2\text{O}_5 \cdot n\text{H}_2\text{O}$) by hydrothermal route [38,39]. In a typical procedure, 2.5 mmol of Nb_2O_5 was added to 18 ml of 3 M KOH solution, which was loaded into 23 mL teflon-lined stainless steel cylindrical autoclave and then heated at 200 °C for 5 hours, a clear solution was obtained. The pH of the solution was made acidic (around 5.5) by dropwise addition of concentrated HCl to precipitate niobic acid, which was filtered and washed several times with distilled water to remove any potassium ions. In the second step freshly prepared niobic acid was added to an aqueous solution of oxalic acid (1M) at 80 °C with constant stirring to obtain milky-white suspension. Then, 2.425 g of bismuth nitrate (5 mmol) was then added to that suspension and the pH of the solution was adjusted to 12 to precipitate as hydroxide by adding 3M KOH solution. The slurry was transferred to 100 mL Teflon-lined stainless steel autoclave up to 80 % of total volume (slurry volume 80 mL). The sealed autoclave was heated at 140 °C for 12 hours and the yellow product was collected by filtration followed by washing with distilled water after natural cooling. Finally the sample was dried in an oven at 80 °C to obtain crystalline BiNbO_4 .

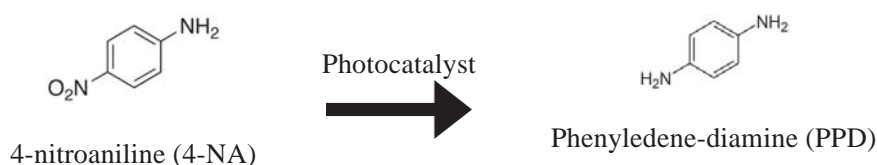
2.2 Structural Characterization

A Bruker-AXS D2 phaser powder diffractometer equipped with a Ni-filtered Cu K α sealed X-ray tube ($\lambda=1.54184$ Å) and a Lynxeye position-sensitive detector was used for X-ray analysis. The PXRD pattern was collected at room temperature and analyzed using the Bruker-AXS EVA software package. The samples were scanned in the 2θ range of 10-70° with a step-size of 0.01° and collection time 0.3 sec at each step. The indexing and refinement were done using TOPAS software. A Perkin Elmer Pyris 1 thermogravimetric analyzer was used to determine the thermal stability and thermal behavior of the compounds prepared. The samples prepared by solution method were heated up to 1000 °C with a temperature ramp of 5 °C/ min under a flow of air. The percent weight loss was calculated relative to the initial weight of the sample to determine the calcination temperature and the thermal stability of the material. Surface areas and pore-size distribution of the samples were determined by nitrogen adsorption-desorption isotherms at liquid nitrogen temperature (77K) using a Quantachrome autosorb-IQ instrument. Prior to the measurements, the samples were outgassed at 120 °C for 2 h under dynamic vacuum. The pore sizes were determined using ASiQwin software. A JEOL 6330 cold field emission Scanning Electron Microscope (SEM) and JEOL 1200 EX Transmission Electron Microscope (TEM) were used to determine the particle size of each of the BiNbO_4 materials. UV-vis diffuse reflectance spectra (DRS) were collected on an Ocean Optics FLAME-S-XR1-ES spectrophotometer equipped with an integrating

sphere. Photoluminescence (PL) spectra were measured at room temperature on fluorescence spectrometer (LS55, PerkinElmer) with an excitation wavelength of 300 nm.

2.3 Photocatalytic test

The reduction of 4-nitroaniline (4-NA) was used as a model reaction (scheme 1) to evaluate the photocatalytic activity of BiNbO₄ catalysts prepared by different methods. The reduction of 4-NA has been chosen as model reaction because of its long-term impact to environment. It is found in wastewater discharges from industries where it is either manufactured or used as an intermediate such as in the synthesis of dyes, antioxidants, pharmaceuticals, in gum inhibitors, poultry medicines, and as a corrosion inhibitor.[42]



Scheme 1: Photocatalytic reduction of 4-nitroaniline (4-NA) to phenylenediamine (PPD)

The photocatalytic reaction was carried out in 80 ml photocatalytic quartz glass cell with 100 mg of BiNbO₄ dispersed in 50 mL of an aqueous solution containing 10 ppm of 4-NA. After adding 10 mg of ammonium oxalate, the suspension was kept under stirring for 1 h in the dark to establish the adsorption-desorption equilibrium. The suspension was then irradiated with visible light ($\lambda \geq 400$ nm). The experiment was carried out under nitrogen atmosphere. Aliquots of 3 mL were taken out every 30 min and centrifuged to remove the solid catalyst particles. Then, the clear solution was analyzed by UV-vis spectroscopy. The 4-NA and PPD concentrations as function of time were determined by measuring the absorbance at 380 nm and 238 nm. The absorbance was converted to concentration using Beer-Lambert law. The photolysis of 4-NA in the presence of hole scavenger ammonium oxalate was also conducted without photocatalyst under visible light irradiation to determine self-induced photodegradation.

3. Results and Discussion

3.1 Characterization:

The phase composition and crystallinity of as-prepared BiNbO₄ were analyzed using PXRD.

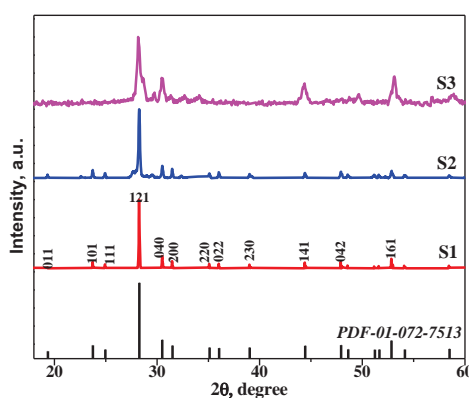


Figure 2: Powder X-ray diffraction analysis of BiNbO₄.

Figure 2 shows the PXRD patterns of BiNbO₄ catalysts synthesized by different methods. The major peaks have been indexed in the orthorhombic phase of BiNbO₄ in the *Pnma* space group (PDF-01-072-7513). The main diffraction peaks in all samples occur at almost the same 2θ positions. It was reported that BiNbO₄ synthesized at temperatures between 750-1030 °C crystallizes in orthorhombic phase. When heated at temperatures higher than 1030 °C, the orthorhombic phase converts to the triclinic phase [40,43]. In the present study, BiNbO₄ was synthesized at temperatures less than 900 °C, which suggests that all samples must correspond to orthorhombic phase. The PXRD of the compound prepared by the hydrothermal method (S3) shows mostly broad diffraction peaks, suggesting less crystallinity and smaller particle size. A summary of refined lattice parameters along with synthetic methods is provided in Table 1.

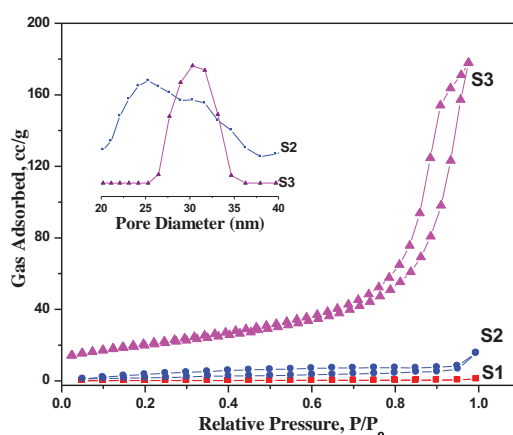


Figure 3: Nitrogen adsorption-desorption isotherms for S1, S2 and S3. The inset picture shows pore size distribution curves for S2 and S3.

Table 1: Textural properties of S1, S2 and S3.

Sample	Synthesis Method	BET Surface Area (m ² g ⁻¹)	Average Pore Size (nm)	Average Particle Size (nm)	Refined Lattice Parameters (Å)
S1	Solid-State Reaction	0.63	-	>1000	$a = 5.6821(2)$ $b = 11.7173(4)$ $c = 4.9558(8)$
S2	Solution Method with P123	5.8	>100	114	$a = 5.649(5)$ $b = 11.5182(2)$ $c = 4.912(4)$
S3	Hydrothermal Method	69.85	37	23	$a = 5.655(4)$ $b = 11.6769(3)$ $c = 4.97113(7)$

The nitrogen adsorption-desorption isotherms were studied to evaluate the surface area and pore size of all BiNbO₄ samples. Typical isotherms for each sample are provided in Figure 3. The surface area and pore size of different samples are provided in Table 1. Typical adsorption-desorption isotherm for sample S3 is of Type IV indicating the mesoporous nature of the sample. In addition, when compared to S1 and S2, the isotherms for S3 show higher absorption at relatively higher pressure ranges ($P/P_0 \sim 1$) suggesting

the formation of large meso-pores. On the other hand, the isotherms indicate that the amount adsorbed by the different samples at low P/P_0 ($P/P_0 < 0.8$) decreases from S3 to S1 at, indicating that pore size increases and specific surface area decreases. The pore size distribution curves for S2 and S3 are shown in the inset in Figure 3. It indicates that sample S3 mainly consists of meso-pores with a peak pore diameter of ca. 37 nm.

To further examine the nature of the particles in each sample, the morphology and microstructure were investigated by electron microscopy. SEM and TEM images of the sample synthesized by solid-state reaction (S1) clearly showed large irregularly shaped particles with sizes in the micrometer range (Figure 4a and d). Similarly, particles size for sample 2 (S2, Figure 4b and d) varies from 90 nm to 138 nm (with average size ~ 114 nm). The larger particles in samples S1 and S2 can be explained on the basis of agglomeration of particles due to the high temperature used in the synthesis of these samples. In contrast the sample synthesized by the hydrothermal method (S3, Figure 4c and f) consists of smooth, spherically shaped particles with average size of ~ 23 nm.

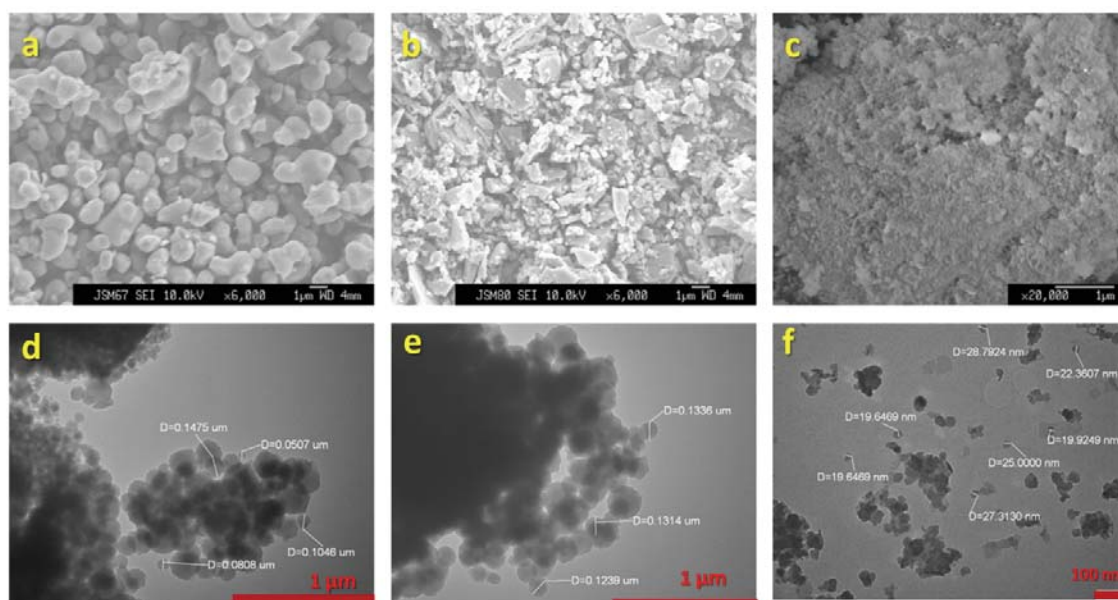


Figure 4: SEM (a, b and c) and TEM (d, e and f) images for BiNbO_4 powders from different synthetic methods.

Figure 5 shows the TGA data of different samples of BiNbO_4 synthesized by wet chemistry routes. The major weight loss ($\sim 75\%$) observed for sample 2 (S2) around 300°C may correspond to the loss of carbon from P123 surfactant. The combination of TGA and PXRD study of S2 clearly show that the crystalline phase of BiNbO_4 is formed only after 700°C . In contrast, TGA of S3 shows negligible weight loss suggesting the presence of pure crystalline phase after the hydrothermal treatment at 140°C .

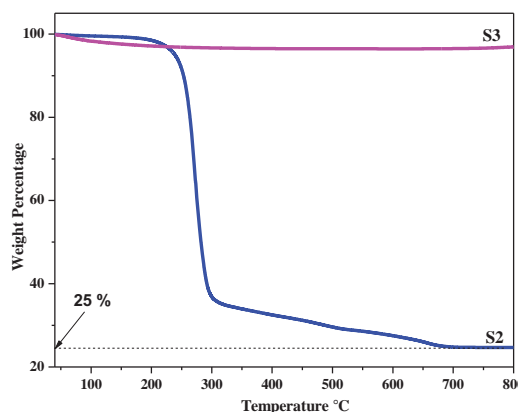


Figure 5: Thermogravimetric analysis of different samples of BiNbO_4 synthesized by wet chemistry route.

Diffuse reflectance UV-vis spectra (Figure 6) show photo-absorption at wavelength shorter than 425 nm, 420 nm, and 414 nm for S1, S2 and S3, respectively. The UV-Vis absorption spectra were transformed from the corresponding diffuse spectra according to the Kubelka-Munk theory to obtain the corresponding band gaps as 2.91 eV, 2.95 eV, and 2.99 eV for S1, S2 and S3, respectively [17]. These results demonstrate that all catalysts in this study may be active in the visible light region ($\lambda \geq 400$ nm).

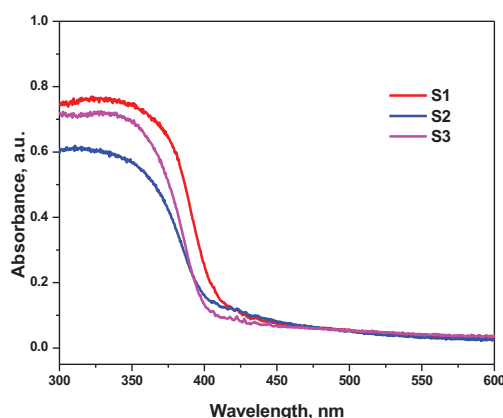


Figure 6: UV-vis diffuse reflectance spectra of different BiNbO_4 samples

3.2. Photocatalytic test

Photocatalytic activities of all samples were evaluated under visible light illumination ($\lambda \geq 400$ nm) using the photocatalytic reduction of 4-NA. For all samples, a decrease of 4-NA absorption intensity at wavelength around 380 nm is observed. As the absorption due to 4-NA decreases, absorptions at 238 and 305 nm corresponding to p-Phenylenedene-diamine (PPD) increases. Figure 7 shows the photocatalytic degradation of 4-NA using different catalysts under visible light irradiation. The photocatalytic decomposition of 4-NA with time depends on the catalyst used. Control experiment (4-NA and $(\text{NH}_4)_2\text{C}_2\text{O}_4$) without catalysts exhibits negligible photocatalytic reduction of 4-NA, which indicates that photolysis of 4-NA can be ignored. The catalysts with higher surface area and small particle size were more catalytically active. Thus S3 reduced all of the 4-NA within 4 hours of visible light irradiation, while only 50 % and 30 % of 4-NA are decomposed by S2 and S1 respectively after the same irradiation time. To check the recyclability of the best active catalyst (S3), we exchanged the solution (after four

hours of photocatalytic reaction) with fresh 4-NA solution and performed the similar photocatalytic experiment for the next 4 hours. It has been found that the degradation efficiency of 4-NA is similar for the second run too. This confirms that those catalysts are very recyclable.

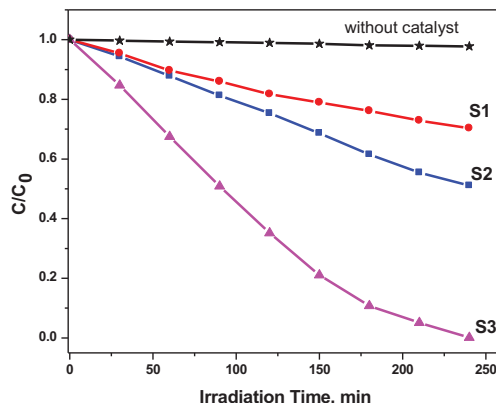


Figure 7: Photoreduction efficiencies of 4-NA as a function of irradiation time by different samples. The absorbance intensity at around 380 nm was used to monitor the concentration of 4-NA. C_0 is the initial concentration of 4-NA, C is the concentration of 4-NA at time t .

The photocatalytic activity results are further supported by photoluminescence (PL) experiments by considering the recombination of photogenerated electron-hole pairs. High photoluminescence intensity generally indicates a high recombination rate of photogenerated charge carriers leading to low efficiency of a given catalyst [16,17,44,45]. Figure 8 shows the PL spectra for different BiNbO₄ samples with an excitation wavelength of 300 nm. The main emission peak is centered at about 325-440 nm for all samples. The PL emission intensity of S3 is significantly smaller than that of S2 and S1, suggesting lower recombination rate of photogenerated charge carriers in S3, which may explain enhanced photocatalytic performance of S3 compared to S1 and S2.

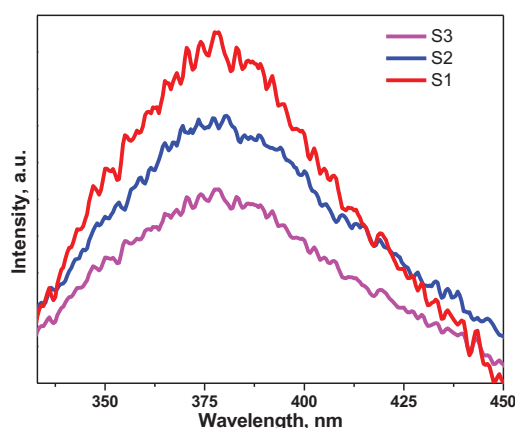


Figure 8: Photoluminescence (PL) spectra for different BiNbO₄ samples.

In the photocatalytic processes, a series of photo-induced reactive species, including h^+ , $\cdot OH$ or $\cdot O_2^-$, take part in the redox process after the electron-hole pairs are generated. In the degradation of 4-NA, the generation of the superoxide radical ($\cdot O_2^-$) is unlikely because all photocatalytic activity processes were conducted under nitrogen flow. Hence, the photogenerated holes (h^+) or $\cdot OH$ are solely responsible for 4-

NA degradation. The holes (h^+) can produce active carbon-dioxide anion radical ($\cdot\text{CO}_2^-$) in the presence of oxalate ($\text{C}_2\text{O}_4^{2-}$) ion. These $\cdot\text{CO}_2^-$ radical anions have a strong reducing ability [46–48].

The photocatalytic degradation of 4-NA was found to follow pseudo-first order kinetics, and can be described by Equation 1.

$$\ln(C_0/C) = -kt \quad (1)$$

where C_0 is the initial concentration of 4-NA, C is the concentration of 4-NA at time t , and k is the rate constant. The corresponding rate constants (k) were calculated and are reported in Table 2. Under similar experimental conditions, the rate constant of 4-NA degradation with S3 was determined to be 3 times larger than that of S2 and 5 times larger than that of S1.

Table 2: Pseudo first order rate constants for photocatalytic degradation process of 4-NA under visible light irradiation ($\lambda \geq 400$ nm).

Sample	4-NA degradation Rate constants (min^{-1})
S1	0.020
S2	0.032
S3	0.098

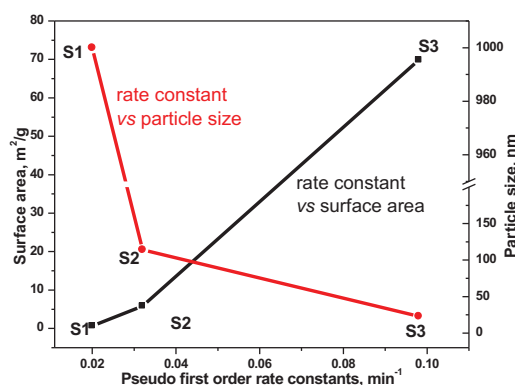


Figure 9: Activity as a function of surface area and particle size

The photocatalytic activity of BiNbO_4 depends on particle size and surface areas as shown in Figure 9. The rate constants of the photocatalytic reduction of 4-NA increases with increasing surface area and decreased with increasing with particle size. S3, which was prepared by hydrothermal method, has the largest surface area ($69.85 \text{ m}^2/\text{g}$) and smallest particle size (23 nm) shows the highest catalytic activity. In contrast S1, which was obtained by high temperature solid state reaction, has the smallest surface area and largest particle size showed the lowest activity. It can be concluded that the size of the particles of BiNbO_4 can affect its photocatalytic efficiency. These results are consistent with previous experimental studies with other type of catalysts [26,49–51]. This may be explained by higher density of active sites as the surface area increases. Moreover, the photogenerated carriers in smaller particles are also likely to transfer more quickly to the sample surface without recombination [24,51].

4. Conclusion

In this work, different bismuth niobate samples with particle sizes ranging from 23-1000 nm were successfully prepared by using different synthetic methods. The photocatalytic activity of each sample was evaluated using the reduction of 4-nitroaniline as model system. The relationship between particle size/ surface area and photocatalytic activity were determined. Samples with smaller particles obtained through hydrothermal methodology have been found to exhibit the highest photocatalytic activity for the degradation of 4-NA under visible-light irradiation. The current study enables an in-depth understanding of the structure–performance relationship of bismuth niobate photocatalyst, which can be applied to other photocatalyst systems.

Acknowledgements

Financial support for this work was provided by the WFU Science Research Fund. The authors would like to thank Dr. Scot Geyer, Wake Forest University, Department of Chemistry, for his help with UV-vis DRS data. The help from Dr. Cynthia Day, Dr. Michael Gross, Zachary Hood, and Baxter Mcguirt is also acknowledged.

References

- [1] Maeda K 2011 Photocatalytic water splitting using semiconductor particles: History and recent developments *J. Photochem. Photobiol. C Photochem. Rev.* **12** 237–68
- [2] Fujishima A and Honda K 1972 Electrochemical Photolysis of Water at a Semiconductor Electrode *Nature* **238** 37–8
- [3] Osterloh F E 2013 Inorganic nanostructures for photoelectrochemical and photocatalytic water splitting *Chem Soc Rev* **42** 2294–320
- [4] Ni M, Leung M K H, Leung D Y C and Sumathy K 2007 A review and recent developments in photocatalytic water-splitting using for hydrogen production *Renew. Sustain. Energy Rev.* **11** 401–25
- [5] Asahi R, Morikawa T, Ohwaki T, Aoki K and Taga Y 2001 Visible-Light Photocatalysis in Nitrogen-Doped Titanium Oxides *Science* **293** 269–71
- [6] Kanhere P and Chen Z 2014 A Review on Visible Light Active Perovskite-Based Photocatalysts *Molecules* **19** 19995–20022
- [7] Liao C-H, Huang C-W and Wu J C S 2012 Hydrogen Production from Semiconductor-based Photocatalysis via Water Splitting *Catalysts* **2** 490–516
- [8] Zhang H, Zong R and Zhu Y 2009 Photocorrosion Inhibition and Photoactivity Enhancement for Zinc Oxide via Hybridization with Monolayer Polyaniline *J. Phys. Chem. C* **113** 4605–11
- [9] Pelaez M, Nolan N T, Pillai S C, Seery M K, Falaras P, Kontos A G, Dunlop P S M, Hamilton J W J, Byrne J A, O'Shea K, Entezari M H and Dionysiou D D 2012 A review on the visible light active titanium dioxide photocatalysts for environmental applications *Appl. Catal. B Environ.* **125** 331–49
- [10] Takata T, Hitoki G, Kondo J N, Hara M, Kobayashi H and Domen K 2007 Visible-light-driven photocatalytic behavior of tantalum-oxynitride and nitride *Res. Chem. Intermed.* **33** 13–25
- [11] Kudo A and Miseki Y 2009 Heterogeneous photocatalyst materials for water splitting *Chem Soc Rev* **38** 253–78

- [12] Ibhaddon A O and Fitzpatrick P 2013 Heterogeneous Photocatalysis: Recent Advances and Applications *Catalysts* **3** 189–218
- [13] Marschall R 2014 Semiconductor Composites: Strategies for Enhancing Charge Carrier Separation to Improve Photocatalytic Activity *Adv. Funct. Mater.* **24** 2421–40
- [14] Wang H, Zhang L, Chen Z, Hu J, Li S, Wang Z, Liu J and Wang X 2014 Semiconductor heterojunction photocatalysts: design, construction, and photocatalytic performances *Chem Soc Rev* **43** 5234–44
- [15] Tahir M and Amin N S 2013 Advances in visible light responsive titanium oxide-based photocatalysts for CO₂ conversion to hydrocarbon fuels *Energy Convers. Manag.* **76** 194–214
- [16] Adhikari S P, Dean H, Hood Z D, Peng R, More K L, Ivanov I, Wu Z and Lachgar A 2015 Visible-light-driven Bi₂O₃/WO₃ composites with enhanced photocatalytic activity *RSC Adv* **5** 91094–102
- [17] Adhikari S P, Hood Z D, More K L, Ivanov I, Zhang L, Gross M and Lachgar A 2015 Visible light assisted photocatalytic hydrogen generation by Ta₂O₅/Bi₂O₃, TaON/Bi₂O₃, and Ta₃N₅/Bi₂O₃ composites *RSC Adv* **5** 54998–5005
- [18] Abe R 2010 Recent progress on photocatalytic and photoelectrochemical water splitting under visible light irradiation *J. Photochem. Photobiol. C Photochem. Rev.* **11** 179–209
- [19] Rajeshwar K 2011 Solar Energy Conversion and Environmental Remediation Using Inorganic Semiconductor–Liquid Interfaces: The Road Traveled and the Way Forward *J. Phys. Chem. Lett.* **2** 1301–9
- [20] Zaleska A 2008 Doped-TiO₂: A Review *Recent Pat. Eng.* **2** 157–64
- [21] Hagfeldt A and Graetzel M 1995 Light-Induced Redox Reactions in Nanocrystalline Systems *Chem. Rev.* **95** 49–68
- [22] Amano F, Ishinaga E and Yamakata A 2013 Effect of Particle Size on the Photocatalytic Activity of WO₃ Particles for Water Oxidation *J. Phys. Chem. C* **117** 22584–90
- [23] Xu N, Shi Z, Fan Y, Dong J, Shi J and Hu M Z-C 1999 Effects of Particle Size of TiO₂ on Photocatalytic Degradation of Methylene Blue in Aqueous Suspensions *Ind. Eng. Chem. Res.* **38** 373–9
- [24] Hagfeldt A and Graetzel M 1995 Light-Induced Redox Reactions in Nanocrystalline Systems *Chem. Rev.* **95** 49–68
- [25] Colmenares J C, Luque R, Campelo J M, Colmenares F, Karpiński Z and Romero A A 2009 Nanostructured Photocatalysts and Their Applications in the Photocatalytic Transformation of Lignocellulosic Biomass: An Overview *Materials* **2** 2228
- [26] Zhang Z, Wang C-C, Zakaria R and Ying J Y 1998 Role of Particle Size in Nanocrystalline TiO₂-Based Photocatalysts *J. Phys. Chem. B* **102** 10871–8
- [27] Zou Z, Ye J and Arakawa H 2001 Optical and structural properties of the BiTa_{1-x}Nb_xO₄ (0 ≤ x ≤ 1) compounds *Solid State Commun.* **119** 471–5

- [28] Zou Z, Ye J and Arakawa H 2003 Photocatalytic water splitting into H₂ and/or O₂ under UV and visible light irradiation with a semiconductor photocatalyst *CANCUN-01* **28** 663–9
- [29] Zhai H-F, Li A-D, Kong J-Z, Li X-F, Zhao J, Guo B-L, Yin J, Li Z-S and Wu D 2013 Preparation and visible-light photocatalytic properties of BiNbO₄ and BiTaO₄ by a citrate method *J. Solid State Chem.* **202** 6–14
- [30] Nisar J, Wang B C, Pathak B, Kang T W and Ahuja R 2011 Mo- and N-doped BiNbO₄ for photocatalysis applications *Appl. Phys. Lett.* **99**
- [31] Wang B C, Nisar J, Pathak B, Kang T W and Ahuja R 2012 Band gap engineering in BiNbO₄ for visible-light photocatalysis *Appl. Phys. Lett.* **100**
- [32] Muktha B, Darriet J, Madras G and Guru Row T N 2006 Crystal structures and photocatalysis of the triclinic polymorphs of BiNbO₄ and BiTaO₄ *J. Solid State Chem.* **179** 3919–25
- [33] Ding K, Chen B, Li Y, Zhang Y and Chen Z 2014 Comparative density functional theory study on the electronic and optical properties of BiMO₄ (M = V, Nb, Ta) *J Mater Chem A* **2** 8294–303
- [34] Zou Z, Ye J, Sayama K and Arakawa H 2001 Photocatalytic and photophysical properties of a novel series of solid photocatalysts, BiTa_{1-x}Nb_xO₄ (0 ≤ x ≤ 1) *Chem. Phys. Lett.* **343** 303–8
- [35] Wang L, Wang W, Shang M, Sun S, Yin W, Ren J and Zhou J 2010 Visible light responsive bismuth niobate photocatalyst: enhanced contaminant degradation and hydrogen generation *J Mater Chem* **20** 8405–10
- [36] Ullah R, Ang H M, Tadé M O and Wang S 2012 Synthesis of doped BiNbO₄ photocatalysts for removal of gaseous volatile organic compounds with artificial sunlight *Chem. Eng. J.* **185–186** 328–36
- [37] Zhang G, Yang J, Zhang S, Xiong Q, Huang B, Wang J and Gong W 2009 Preparation of nanosized Bi₃NbO₇ and its visible-light photocatalytic property *J. Hazard. Mater.* **172** 986–92
- [38] Min Y, Zhang F-J, Zhao W, Zheng F, Chen Y and Zhang Y 2012 Hydrothermal synthesis of nanosized bismuth niobate and enhanced photocatalytic activity by coupling of graphene sheets *Chem. Eng. J.* **209** 215–22
- [39] Hou J, Cao R, Wang Z, Jiao S and Zhu H 2012 Hierarchical nitrogen doped bismuth niobate architectures: Controllable synthesis and excellent photocatalytic activity *J. Hazard. Mater.* **217–218** 177–86
- [40] Dunkle S S and Suslick K S 2009 Photodegradation of BiNbO₄ Powder during Photocatalytic Reactions *J. Phys. Chem. C* **113** 10341–5
- [41] Yang P, Zhao D, Margolese D I, Chmelka B F and Stucky G D 1998 Generalized syntheses of large-pore mesoporous metal oxides with semicrystalline frameworks *Nature* **396** 152–5
- [42] Gautam S, Kamble S P, Sawant S B and Pangarkar V G 2005 Photocatalytic degradation of 4-nitroaniline using solar and artificial UV radiation *Chem. Eng. J.* **110** 129–37

- [43] Zhou D, Wang H, Yao X, Wei X, Xiang F and Pang L 2007 Phase transformation in BiNbO₄ ceramics *Appl. Phys. Lett.* **90**
- [44] Du Y, Zhao L and Zhang Y 2014 Roles of TaON and Ta₃N₅ in the visible-Fenton-like degradation of atrazine *J. Hazard. Mater.* **267** 55–61
- [45] Mayer M T, Du C and Wang D 2012 Hematite/Si Nanowire Dual-Absorber System for Photoelectrochemical Water Splitting at Low Applied Potentials *J. Am. Chem. Soc.* **134** 12406–9
- [46] Wu W, Lin R, Shen L, Liang R, Yuan R and Wu L 2013 Visible-light-induced photocatalytic hydrogenation of 4-nitroaniline over In₂S₃ photocatalyst in water *Catal. Commun.* **40** 1–4
- [47] Imamura K, Iwasaki S, Maeda T, Hashimoto K, Ohtani B and Kominami H 2011 Photocatalytic reduction of nitrobenzenes to aminobenzenes in aqueous suspensions of titanium(IV) oxide in the presence of hole scavengers under deaerated and aerated conditions *Phys Chem Chem Phys* **13** 5114–9
- [48] Wu W, Liu G, Liang S, Chen Y, Shen L, Zheng H, Yuan R, Hou Y and Wu L 2012 Efficient visible-light-induced photocatalytic reduction of 4-nitroaniline to p-phenylenediamine over nanocrystalline PbBi₂Nb₂O₉ *J. Catal.* **290** 13–7
- [49] Dodd A C, McKinley A J, Saunders M and Tsuzuki T 2006 Effect of Particle Size on the Photocatalytic Activity of Nanoparticulate Zinc Oxide *J. Nanoparticle Res.* **8** 43–51
- [50] Amano F, Nogami K, Tanaka M and Ohtani B 2010 Correlation between Surface Area and Photocatalytic Activity for Acetaldehyde Decomposition over Bismuth Tungstate Particles with a Hierarchical Structure *Langmuir* **26** 7174–80
- [51] Li X, Li Q and Wang L 2013 The effects of NaNbO₃ particle size on the photocatalytic activity for 2-propanol photodegradation *Phys Chem Chem Phys* **15** 14282–9